Effects of Free Convection on Three-Dimensional Protein Transport in Hollow-Fiber Bioreactors

Marek Łabęcki and James M. Piret
Dept. of Chemical and Biological Engineering, and Biotechnology Laboratory,
University of British Columbia, Vancouver, BC V6T 1Z4, Canada

Bruce D. Bowen
Dept. of Chemical and Biological Engineering, University of British Columbia, Vancouver, BC V6T 1Z4, Canada

DOI 10.1002/aic.10159
Published online in Wiley InterScience (www.interscience.wiley.com).

A three-dimensional analysis of protein redistribution in the extracapillary space (ECS) of ultrafiltration membrane hollow-fiber bioreactors (HFBRs), used for mammalian cell culture, is presented. Homogeneous distribution of growth-factor proteins in the ECS is essential for a successful startup and efficient operation of HFBRs. The ECS protein transport under most startup conditions of practical interest is strongly influenced by gravity and represents a complex interaction of forced- and free-convective phenomena. These effects were investigated using a comprehensive porous medium model (PMM) that accounts for local variations of fluid density, fluid viscosity, and osmotic pressure resulting from time-dependent changes in the protein concentration field. In addition, the model considers the influence of fiber-free manifolds, which are adjacent to the fiber bundle and are accessible to ECS proteins and cells. The PMM predictions of the ECS protein distributions at different bioreactor orientations were in good agreement with the observed distributions of a colored test protein in an experimental HFBR cartridge. The results of this study can provide useful insights for optimizing HFBR operation strategies.
© 2004 American Institute of Chemical Engineers *AIChE J,* 50: 1974–1990, 2004
Keywords: hollow-fiber membranes, hollow-fiber bioreactors, mammalian cell culture, porous medium model, free convection

Introduction

The field of mammalian cell culture in hollow-fiber bioreactors (HFBRs) has been undergoing a dynamic expansion in recent decades. For small-scale production of diagnostic monoclonal antibodies (MAbs), HFBR technology has become a viable alternative to ascites tumors in mice (Jackson et al., 1996). More recently, application of HFBRs as extracorporeal bioartificial organs has been growing rapidly. For example, multiple liver assist devices relying on hollow-fiber culture of hepatocytes (HepatAssist, ELAD, LIVERx2000, BLSS, and MELS) (Allen et al., 2001), as well as a hollow-fiber renal assist device (RAD) hosting kidney cells (Humes et al., 2002), are in various stages of clinical evaluation. HFBRs have also been successfully used to grow therapeutic cells, such as the human tumor-infiltrating lymphocytes for use in cancer patients (Malone et al., 2001).

Numerous HFBR designs have been proposed (Tharakan et al., 1988), but the most conventional option involves entrapment of mammalian cells in the extracapillary space (ECS), or shell side, of a cylindrical cartridge densely packed with hollow fibers that are fixed at both ends in an epoxy support (Łabęcki et al., 1995). Recirculation flow of medium through the fiber lumina, or intracapillary space (ICS), allows exchange of oxygen as well as small nutrients and metabolites with the ECS, thus providing the cells with stable growth conditions. A

Correspondence concerning this article should be addressed to J. M Piret at jpiret@chml.ubc.ca.

© 2004 American Institute of Chemical Engineers

typical cartridge possesses two annular, fiber-free regions that extend over about 10% of the axial length from either end of the ECS. These regions, referred to as the *ECS manifolds*, are used to inoculate the bioreactor and to harvest the product protein through the adjacent ECS ports. The presence of manifolds often complicates bioreactor operation by trapping some of the cells (Lee et al., 2003) and proteins (Łabęcki et al., 2001).

One of the most important factors in a successful HFBR operation is the establishment of uniform cell growth conditions in the ECS. In particular, the spatial homogeneity of growth-factor protein distributions in the ECS is critical to the success and efficiency of the cell or tissue engineering culture. The distribution of cells in the ECS has been shown to follow the distribution of growth-factor proteins (Piret and Cooney, 1990), although an exact correlation between these two is difficult to determine and quantify. Nonetheless, an analysis of ECS protein distributions may serve to indicate where the ECS cells will proliferate, at least during the early stages of bioreactor operation (that is, at low cell densities in the ECS). This could also facilitate identification of critical factors and conditions potentially leading to cell culture failure during HFBR start-up.

In many HFBR configurations, both ECS ports remain closed during much of the culture run, and the corresponding flow configuration is termed the *closed-shell mode*. In this case, the axial pressure gradient in the ICS, in the presence of the membranes, induces a secondary flow in the ECS, also referred to as Starling flow (Starling, 1896). As a consequence, proteins and cells can be convectively carried to the downstream end of the ECS (Piret and Cooney, 1990; Waterland et al., 1975), which may lead to spatial heterogeneities in the growth environment and hence deterioration of the bioreactor performance. In addition, the ECS proteins in horizontal HFBRs have been shown to become polarized toward the bottom of the cartridge by the action of gravitational forces (Piret and Cooney, 1990). The ECS heterogeneity problem has to some extent been overcome in an HFBR system developed by Cellex (formerly Endotronics), where the ECS contents are periodically flushed into an external expansion chamber (Gramer et al., 1999).

Previous theoretical analyses of HFBR fluid flow and protein transport can be generally divided into two groups, corresponding to two distinct modeling approaches. The Krogh cylinder models (KCMs) are based on the assumption that the fluid flow and mass transfer phenomena in the HFBR can be analyzed using a representative single-fiber unit, the Krogh cylinder (Krogh, 1919). Limitations of this assumption in the presence of transverse pressure or concentration gradients in the bioreactor stimulated the development of the two-dimensional porous medium model (PMM) (Łabęcki et al., 1995, 1996). In this approach, the intra- and extracapillary spaces of the fiber bundle are treated as two interpenetrating porous media with uniformly distributed sinks and sources of fluid. The PMM domain is defined around the entire bundle of fibers, rather than a single fiber, thus providing a more realistic description of the HFBR.

Initial theoretical studies of HFBRs used the KCM approach and concentrated mainly on the modeling of the distribution and consumption of low molar mass (low-MM) substrates, perceived as critical to cell growth and product generation (Kim and Cooney, 1976; Piret and Cooney, 1991; Rony, 1971; Waterland et al., 1974; Webster and Shuler, 1978). An interest in understanding the role of fluid flow in HFBRs was stimulated by anticipation that convection might help alleviate potential problems of substrate limitation, metabolite inhibition, or growth heterogeneities. In reactors equipped with highly permeable membranes [such as microporous or ultrafiltration membranes with high molar mass cutoffs (MMCOs)], small proteins can pass unhindered between the ECS and the ICS, and their distributions can be described using models similar to those developed for low-MM solutes. More recently, it has become clear that the distribution of larger proteins (growth factors, growth inhibitors, or products) in ultrafilter hollow fibers can be as important to efficient bioreactor operation as the transport of low-MM solutes. Because of the much lower diffusivities of these ECS proteins, and the fact that their passage through the membrane is either hindered or completely inhibited, a meaningful model formulation should include ECS convection or at least its axial component. This has been appreciated by Salmon et al. (1988) and by Pillarella and Zydney (1990), although their models did not consider the influence of osmotic pressure or gravity on protein distribution.

The first KCM formulation that included a concentration-dependent osmotic term in the ECS fluid flow equations was presented by Taylor et al. (1994). Their simulations of ECS protein transport in closed-shell HFBRs showed that a neglect of the osmotic term would lead to unrealistic protein distributions, such as with all of the protein packed to an extremely high concentration within a very thin layer at the downstream end of the ECS. Subsequent experimental as well as theoretical investigations confirmed the importance of osmotic effects for a variety of HFBR protein transport conditions, both in closed-shell [KCM studies by Patkar et al. (1995), Koska et al. (1997), and Łabęcki et al. (1998)] and in open-shell configurations [PMM study by Łabęcki et al. (1996)].

The neglect of gravitational effects represents a remaining, significant limitation of the previous KCM and PMM formulations, which cannot provide a reliable description of HFBR protein transport for different reactor orientations, especially for nonvertical or upflow cartridges. Natural-convective instabilities and their beneficial effects on ultrafiltration performance have been described for flat membranes (Youm et al., 1996), but not for hollow-fiber systems. The aim of the present study was to eliminate this shortcoming by including buoyancy terms in the equations and formulating the PMM in three spatial dimensions. Moreover, the model has been extended to account for the presence of fiber-free ECS manifolds, which constitute a significant portion of the total volume accessible to the protein. The resulting three-dimensional (3-D) PMM is an advanced simulation tool capable of a much more realistic analysis of protein transport in closed-shell HFBRs. The overall trends of model-generated ECS protein distributions at different bioreactor orientations are consistent with those observed in experimental HFBR cartridges, which justifies the use of the 3-D PMM for predictive purposes.

Model Development

Underlying assumptions

The HFBR protein transport model proposed here is an extension of the two-dimensional PMM described elsewhere (Łabęcki et al., 1995, 1996). The most important new features of this extension are the addition of angular position as another

spatial dimension, addition of density and viscosity gradients, and the inclusion of the ECS manifold effects. As before, the ICS and the ECS of the hollow-fiber bundle are treated as two interpenetrating porous media, with the governing equations formulated in a coupled form for both of these regions. In the present analysis, the membranes are assumed impermeable to protein, although the general model formulation does allow for transmembrane protein transport (Łabęcki et al., 1998). Only the closed-shell reactor configuration is considered. A detailed list of the model assumptions is as follows.

(1) Fluid flow and protein transport are unaffected by the presence of cells in the ECS. This approximation is valid during the HFBR startup phase, when the ECS cell density is low. Cells are absent from the ICS.

(2) The HFBR system is isothermal.

(3) The ECS porous medium is inhomogeneous with respect to fluid density and viscosity, which depend on protein concentration and hence can vary with position within the ECS. The ICS porous medium is assumed to have a constant protein concentration and thus is homogeneous with respect to fluid density and viscosity. The porosity within each of the two spaces is constant.

(4) The fluid is incompressible and Newtonian. The incompressibility assumption is also valid for variable fluid density, as long as the latter is a linear function of protein concentration. As a consequence of the incompressibility assumption, the system hydrodynamics are always quasi-steady (that is, the flow field responds instantaneously to any transient changes in protein concentration distribution).

(5) The ECS fluid flow is characterized by low Reynolds numbers (Re $<$ 1), making Darcy's law applicable to the ECS region. The bulk ICS fluid flow (that is, the ICS flow averaged over many fibers) is laminar, locally fully developed, and essentially one-dimensional in the direction of the cartridge axis; thus it can also be described using an expression similar to Darcy's law.

(6) Dispersive protein fluxes attributed to local fluctuations in the ECS velocities are neglected, relative to the fluxes resulting from locally averaged flows.

(7) The ECS porous medium is anisotropic with respect to the Darcy permeability and protein diffusivity; that is, these properties are assumed to depend on direction within the ECS. The radial and angular components of each of these two properties are equal (except when the HFBR cartridge is oriented vertically; see next assumption).

(8) For nonvertical orientations, planar symmetry of the system is assumed, with the symmetry plane cutting through the reactor diameter and being parallel to the gravity vector. For the vertical orientation, axial symmetry about the reactor's longitudinal axis is assumed. In the latter case, the angular components of the Darcy permeability and protein diffusivity are set to zero, to reflect the absence of net fluid and solute fluxes in the angular direction.

(9) The membrane hydraulic permeability L_p, fiber dimensions, as well as all components of the Darcy permeability and protein diffusivity tensors, are constant in space and in time.

Fluid dynamics

The equations governing the ICS and ECS hydrodynamics are derived by combining the Darcy and continuity laws for each of the two regions. The continuity equation for an incompressible, inhomogeneous fluid in the ECS porous medium, with velocity fluctuations neglected, has the following form (Bear, 1972, p. 103)

$$\varepsilon_S \frac{\partial \rho_S}{\partial t} + \nabla(\rho_S \mathbf{v}_S) = \rho_0 A_V J_{TMF} \tag{1}$$

where A_V is the membrane surface area per unit volume of the reactor, and the righthand side term is the transmembrane fluid exchange expressed as a spatially distributed source/sink. The transmembrane fluid flux J_{TMF} is calculated as

$$J_{TMF} = \frac{L_p}{\mu_0}(P_L - P_S - \Delta\Pi_{eff}) \tag{2}$$

with the effective osmotic pressure difference, for a single protein that is completely rejected by the membranes, expressed as follows

$$\Delta\Pi_{eff} = \Pi_L - \Pi_S \tag{3}$$

where Π_L and Π_S are evaluated as a function of protein concentration on the lumen and shell sides of the membrane, respectively. Expansion of Eq. 1 in cylindrical coordinates yields

$$\varepsilon_S \frac{\partial \rho'_S}{\partial t} + \nu_{S,r}\frac{\partial \rho'_S}{\partial r} + \frac{\nu_{S,\theta}}{r}\frac{\partial \rho'_S}{\partial \theta} + \nu_{S,z}\frac{\partial \rho'_S}{\partial z} + \rho'_S\left[\frac{1}{r}\frac{\partial (r\nu_{S,r})}{\partial r} + \frac{1}{r}\frac{\partial \nu_{S,\theta}}{\partial \theta} + \frac{\partial \nu_{S,z}}{\partial z}\right] = A_V J_{TMF} \tag{4a}$$

where $\rho'_S = \rho_S/\rho_0$ is the dimensionless ECS fluid density. By comparison, the corresponding homogeneous continuity equation for the ECS is

$$\rho'_S\left[\frac{1}{r}\frac{\partial (r\nu_{S,r})}{\partial r} + \frac{1}{r}\frac{\partial \nu_{S,\theta}}{\partial \theta} + \frac{\partial \nu_{S,z}}{\partial z}\right] = A_V J_{TMF} \tag{4b}$$

For the ICS, where the fluid is homogeneous and the flow is essentially 1-D in the z-direction, the continuity law becomes

$$-\rho'_L \frac{\partial \nu_{L,z}}{\partial z} = A_V J_{TMF} \tag{5}$$

The general form of Darcy's law for a control volume (CV) located in an inhomogeneous porous medium is (Bear, 1972, p. 106)

$$\nu_i = -\frac{k_i}{\mu}\left(\frac{\partial P}{\partial x_i} + \rho g \frac{\partial h}{\partial x_i}\right) \tag{6}$$

where x_i denotes an independent spatial variable and h is the elevation of the CV center of mass above a datum level. For a cylindrical bioreactor cartridge, $x_i = r$, θ, or z, and the datum

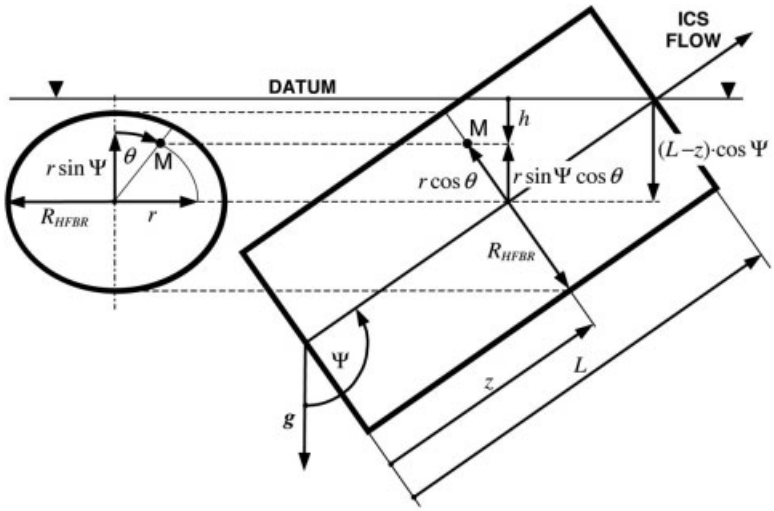

Figure 1. Spatial arrangement of variables and parameters in a cylindrical domain of the 3-D HFBR porous medium model (dimensions not to scale).

The thick line marks the boundary of the fiber bundle in a cross section through point M (r, θ, z) (left) and in a longitudinal section through the cartridge centerline (right). $h = r \sin \Psi \cos \theta + (L - z)\cos \Psi$ is the elevation of point M relative to the datum level; Ψ is the angle between the vector of gravitational acceleration (g) and the direction of ICS flow.

level is set as the center of the outlet area, that is, at $r = 0$ and $z = L$. Hence, the elevation h is calculated as

$$h = r \sin \Psi \cos \theta + (L - z)\cos \Psi \tag{7}$$

where Ψ is the cartridge inclination angle, defined as the angle between the direction of bulk ICS flow and the direction of the gravity vector, and θ is the angular position measured from the highest point of a given circular cross section (Figure 1). [Note that for vertical cartridges θ becomes irrelevant because of axial symmetry. The formalism presented here is valid for all cartridge orientations (that is, for all Ψ).] The Darcy Eq. 6 for the ECS and ICS can be more conveniently formulated in terms of the piezometric pressure $\hat{P} = P + \rho_0 g h$ and the reduced density $\Delta\rho = \rho - \rho_0$, as

$$\nu_{S,r} = -\frac{k_{S,r}}{\mu_S}\left(\frac{\partial \hat{P}_S}{\partial r} + \Delta\rho_S g \sin \Psi \cos \theta\right) \tag{8a}$$

$$\nu_{S,\theta} = -\frac{k_{S,\theta}}{\mu_S}\left(\frac{1}{r}\frac{\partial \hat{P}_S}{\partial \theta} - \Delta\rho_S g \sin \Psi \sin \theta\right) \tag{8b}$$

$$\nu_{S,z} = -\frac{k_{S,z}}{\mu_S}\left(\frac{\partial \hat{P}_S}{\partial z} - \Delta\rho_S g \cos \Psi\right) \tag{8c}$$

and

$$\nu_{L,z} = -\frac{k_{L,z}}{\mu_L}\left(\frac{\partial \hat{P}_L}{\partial z} - \Delta\rho_L g \cos \Psi\right) \tag{9}$$

The HFBR fluid flow equations are obtained by inserting the velocity expressions, Eqs. 8 and 9, into the respective continuity Eqs. 4a and 5, which eventually leads to

$$A_{r2}\frac{1}{r}\frac{\partial}{\partial r}\left(r\frac{\partial \hat{P}_S}{\partial r}\right) + A_{r1}\frac{\partial \hat{P}_S}{\partial r} + A_{\theta 2}\frac{1}{r}\frac{\partial^2 \hat{P}_S}{\partial \theta^2} + A_{\theta 1}\frac{1}{r}\frac{\partial \hat{P}_S}{\partial \theta} + A_{z2}\frac{\partial^2 \hat{P}_S}{\partial z^2} + A_{z1}\frac{\partial \hat{P}_S}{\partial z} + \hat{P}_S - \hat{P}_L = A_S \tag{10}$$

and

$$A_{L2}\frac{\partial^2 \hat{P}_L}{\partial z^2} - \hat{P}_L + \hat{P}_S = A_L \tag{11}$$

where the parameters A depend locally on fluid density, fluid viscosity, and osmotic pressure (see Appendix). The $1/r$ factor has been preserved in some of the terms in Eq. 10 for convenience during numerical discretization because the integration over a cylindrical elementary volume requires multiplication of the integrand terms by r.

The boundary conditions for the ECS Eq. 10 are generally derived by demanding that the normal velocity components become zero at all impermeable boundaries (except at $r = 0$). Symmetry with respect to the $\theta = 0$ and $\theta = \pi$ planes is assumed for nonvertical cartridges ($\Psi < 180°$), whereas axial symmetry about the $r = 0$ line is assumed in the vertical case ($\Psi = 180°$). At $r = 0$, the condition becomes immaterial, because the mass flow through this degenerate one-dimensional boundary is zero. For simplicity, the outer radial boundary ($r = R_{\mathrm{HFBR}}$) is treated as impermeable over its whole length, that is, including the upstream and downstream segments where the fiber bundle adjoins the ECS manifolds (Łabęcki et al., 1995, 1996). For the ICS Eq. 11, a known axial velocity, $v_{L,in}$, is specified at the lumen inlet, and a known value of the piezometric pressure, $\hat{P}_{L,out}$, is set at the lumen outlet. Both $v_{L,in}$ and $\hat{P}_{L,out}$ are assumed constant over the cartridge cross section (note that, by definition, $\hat{P}_{L,out}$ does not vary with h). Alterna-

tively, a known and constant $\hat{P}_{L,in}$ can be specified at the inlet, although the velocity condition is more consistent with the standard HFBR system configuration in which a peristaltic pump circulates the liquid through the cartridge at an essentially constant ICS flow rate.

ECS protein transport

The three-dimensional distribution of protein in the ECS (with the neglect of dispersive fluxes arising from local velocity fluctuations) is described using a transient convection–diffusion equation, that is

$$\varepsilon_S \frac{\partial C_S}{\partial t} = \frac{1}{r}\frac{\partial (rJ_{P,r})}{\partial r} + \frac{1}{r}\frac{\partial J_{P,\theta}}{\partial \theta} + \frac{\partial J_{P,z}}{\partial z} + A_V J_{TMP} \quad (12)$$

where C_S is the local interstitial protein concentration (that is, mass of protein per unit volume of the ECS). For a leaking protein, equations derived elsewhere (Łabęcki et al., 1998) are available to model the transmembrane flux, J_{TMP}, and its effect on the ICS concentration. In the present analysis, the protein is assumed to be completely retained in the ECS or ICS, and hence J_{TMP} is set to zero. Upon expansion of the ECS protein fluxes (J_P) into diffusive and convective components, the following equation governing ECS protein transport is obtained

$$\varepsilon_S \frac{\partial C_S}{\partial t} = \frac{1}{r}\frac{\partial}{\partial r}\left(rD_{S,r}\frac{\partial C_S}{\partial r} - r\nu_{S,r}C_S\right) + \frac{1}{r}\frac{\partial}{\partial \theta}\left(\frac{D_{S,\theta}}{r}\frac{\partial C_S}{\partial \theta} - \nu_{S,\theta}C_S\right) + \frac{\partial}{\partial z}\left(D_{S,z}\frac{\partial C_S}{\partial z} - \nu_{S,z}C_S\right) \quad (13)$$

where $v_{S,r}$, $v_{S,\theta}$, and $v_{S,z}$ are the superficial ECS velocity components expressed by the system Eqs. 8a–8c. Equation 13 is coupled with the hydrodynamic Eqs. 10 and 11 through the fluid velocities, which themselves are influenced by the protein distribution through the concentration-dependent density, viscosity, and osmotic pressure. The boundary conditions for Eq. 13 are similar to those for the ECS fluid flow Eq. 10. The axial and radial boundaries ($z = 0$, $z = L$, $r = 0$, and $r = R_{\mathrm{HFBR}}$) are treated as impermeable, whereas planar symmetry is assumed at $\theta = 0$ and $\theta = \pi$. The initial condition is a known ECS concentration distribution at time $t = 0$. In this study, the starting protein concentration was always assumed spatially constant and equal to C_0 throughout the ECS, including the manifolds.

ECS manifolds

Considering the significant role of the ECS manifolds observed in the earlier experimental studies of ECS protein redistribution (Łabęcki et al., 1996, 1998; Patkar et al., 1995), it is clear that these regions should be included in any realistic HFBR model, even if only in an approximate manner. A rigorous hydrodynamic description of the manifolds, even in the closed-shell case, would require inclusion of shear stress terms in the equations as well as iteration of the manifold pressure and velocity solutions at each time step. In addition, because the fluid flow and protein distributions must be matched at the boundary between the manifold and the fiber bundle, equations of the same order (that is, second-order) would have to be used for both of these regions. Thus, the model complexity would increase significantly.

To avoid these complications, a simpler approach to the modeling of the manifolds has been adopted here by implementing the following ECS concentration adjustment scheme. The space occupied by each ECS manifold was subdivided into a 3-D mesh of control volumes (CVs). At each time step, the protein was assumed to equilibrate instantaneously between the radially outermost layer of CVs in the fiber bundle and the adjacent layer of CVs in each ECS manifold (which is essentially a simplified view of the manifold-bundle protein exchange by radial diffusion). The equilibration was performed by artificially redistributing the protein between two neighboring CVs, such that the adjusted concentrations were the same in both CVs. In addition, a similar equilibration of the protein was performed between any two neighboring CVs within the manifold, as long as their concentrations were different and the center of the higher-concentration CV was above or at the same level as the center of the lower-concentration CV. This effectively means that the concentration in each manifold was never allowed to increase with position upward or horizontally, given that the existence of such concentration gradients would be expected to induce free-convective protein redistribution within the manifold.

Table 1. Parameters for the 3-D HFBR Model

Parameter	Value
n	8128
R_L	1.09×10^{-4} m
R_F	1.24×10^{-4} m
R_{HFBR}	0.01575 m
L	0.215 m
z_m	0.021 m
V_m	13.6 cm^3
ε_S	0.4423
A_V	7907.1 m^{-1}
L_p	7×10^{-15} m
$k_{L,z}$	5.23×10^{-10} m^2
$k_{S,z}$	9.39×10^{-10} m^2
$k_{S,r}$	2.01×10^{-10} m^2
$k_{S,\theta}$	2.01×10^{-10} m^2
T	310 K (37°C)
M	69 kg mol^{-1}
$A_{\Pi 1}$	10.473×10^{-3} m^3 kg^{-1}
$A_{\Pi 2}$	17.374×10^{-6} m^6 kg^{-2}
ρ_0 (310 K)	993.45 kg m^{-3}
μ_0 (310 K)	6.9164×10^{-4} Pa s^{-1}
$A_{\mu 1}$	3.8×10^{-3} m^3 kg^{-1}
$A_{\mu 2}$	2.2×10^{-5} m^6 kg^{-2}
D_A (293 K)	6.9×10^{-11} m^2 s^{-1}
$D_{S,z}$ (310 K)	3.82×10^{-11} m^2 s^{-1}
$D_{S,r}$ (310 K)	3.00×10^{-11} m^2 s^{-1}
$D_{S,\theta}$ (310 K)	3.00×10^{-11} m^2 s^{-1}

Model parameters

The major model parameters are listed in Table 1. The fiber dimensions and other cartridge-specific parameters pertain to the Gambro GFE-15 hollow-fiber module described elsewhere (Łabęcki et al., 1995; Patkar et al., 1995). The cell-free ECS porosity ϵ_S and the membrane surface area per unit volume A_V

were evaluated from the cartridge and wet fiber dimensions, as before (Łabęcki et al., 1995). The ECS volume was calculated to be 74.1 cm^3, and the fiber-free volume for each ECS manifold about 13.6 cm^3 (based on the outer manifold radius of 0.0206 m). The axial ICS and ECS hydraulic permeabilities $k_{L,z}$ and $k_{S,z}$ and the membrane permeability L_p were estimated from earlier measurements (Łabęcki et al., 1998). The radial and angular ECS permeabilities $k_{S,r}$ and $k_{S,\theta}$ were assumed to be equal and were calculated using a formula derived by Happel (1959) for flow across a bank of cylinders (Łabęcki et al., 1996).

The protein properties were all assumed to be the same as those for BSA. The fluid density varied with protein concentration according to the following experimental formula obtained by Vilker et al. (1981) and valid for BSA concentrations up to 580 kg/m^3

$$\rho = \rho_0 + C(1 - \rho_0/\rho_A) \tag{14}$$

where $\rho_A = 1340$ kg/m^3. The relationship between fluid viscosity and protein concentration was taken to be (Anderson et al. 1978)

$$\mu = \mu_0(1 + A_{\mu 1}C + A_{\mu 2}C^2) \tag{15}$$

valid for BSA solutions in 0.1 M KCl at pH $\approx$ 6.5. The protein-free fluid density ρ_0 and viscosity μ_0 were assumed to be the same as for pure water and to depend on temperature as

$$\rho_0\,[kg/m^3] = 999.86 + 0.06T - 7.74 \times 10^{-3}T^2 + 3.88 \times 10^{-5}T^3 \tag{16}$$

and

$$\log\left(\frac{\mu_0}{1.0021 \times 10^{-3}}\right) = \frac{1.3272(20 - T) - 0.001053(20 - T)^2}{T + 105} \tag{17}$$

where T is in °C, and 1.0021×10^{-3} Pa s^{-1} is the water viscosity at 293 K (20°C). Equation 16 was obtained as a best cubic fit of tabulated data given in Perry and Green (1984, 3-75), and formula 17 was taken from Weast (1975, F-49). The osmotic pressure Π was calculated as a function of protein concentration C and temperature T, using (Patkar et al., 1995)

$$\Pi = \frac{R_g T}{M} C(1 + A_{\Pi 1}C + A_{\Pi 2}C^2) \tag{18}$$

The free-fluid protein diffusivity D was obtained by extrapolation of the BSA diffusivity at 293 K (20°C), $D_A = 6.9 \times 10^{-11}$ m^2/s (van den Berg and Smolders, 1989), to temperature T, with $D\mu/T$ assumed constant. The axial and radial components of ECS protein diffusivity were calculated from D as before (Łabęcki et al., 1996), with the angular component $D_{S,\theta} = D_{S,r}$. Because diffusion plays a relatively insignificant role here, and because the BSA diffusivity changes very little with protein concentration (Anderson et al., 1978), spatial variations of D were neglected.

Numerical Techniques

Solution of the pressure and concentration equations

Discretization of the hydrodynamic Eqs. 10 and 11 was performed by integration over a 3-D cylindrical CV (Patankar, 1980). A finite-difference, uniform grid was used in each spatial dimension. A 7-point formula was used, with each point of the domain affected only by its immediate neighbors in each direction. The pressures were evaluated at the centers of the CVs, and the velocities at the centers of the CV faces, halfway between the pressure nodes. Within each CV, all of the A coefficients in Eqs. 10 and 11 were treated as spatially constant, and the pressure derivatives over one spatial variable were assumed constant over the remaining two variables. The discretization procedure produced a set of linear algebraic equations with the local ICS and ECS pressures as unknowns and with coefficients varying in time and space through their dependence on protein concentration. These equations were solved at each time step, always using the most recent ECS concentration values to update the coefficients.

The ECS pressure distributions were obtained by a direct solution using the Gauss elimination method (Tannehill et al., 1997, p. 148), appropriately modified so as to avoid excessive use of computational memory resulting from the storage of redundant zero elements. The ICS pressure Eq. 11 was solved iteratively using the explicit Gauss–Seidel point algorithm (Tannehill et al., 1997, p. 148). Attempts to use the same method for the solution of the ECS problem (Eq. 10) were eventually abandoned because of numerical difficulties, including (1) unpredictable convergence behavior and stalling; (2) strong dependence of the solution convergence on grid size; and (3) development of artificial pressure gradients in the direction of point update.

The ECS protein concentration equation (Eq. 13) was solved using a 3-D formulation of the alternate direction implicit (ADI) method (Douglas, 1962), combined with the hybrid scheme proposed by Patankar (1980) for upwinding control. For comparison, the ECS concentration problem was also solved by a direct solver using the modified Gauss elimination routine described above. Both approaches yielded virtually identical solutions (within 4 significant digits), but the ADI method was computationally more efficient than the direct solver. Numerical tests verified that, in the absence of gravity and angular gradients in the HFBR, the results generated using the present 3-D model and numerical code were consistent with the predictions of the 2-D HFBR porous medium model and a 1-D Krogh cylinder model developed earlier (Łabęcki et al., 1996).

Input and output

The most important operating parameters varied in this study were (1) the cartridge inclination angle relative to the gravity vector (Ψ); (2) the inlet ICS flow rate (Q_L); and (3) the average ECS protein concentration (C_0). The inlet ICS flow rate was 14.2 cm^3/s (850 mL/min) in the simulations of experimental runs and 10 cm^3/s (600 mL/min) in most other cases (lower values were also used to investigate the effect of Q_L). The ICS

was normally assumed to be protein-free, given that the effect of the mixing-cup ICS protein concentration (C_L) on the results was found to be negligible. The temperature was taken to be 310 K (37°C), except in the simulations of room-temperature experiments. The outlet ICS piezometric pressure $\hat{P}_{L,out}$ was set to zero.

In most simulations, $N_i = 50$ axial, $N_j = 10$ radial, and $N_k = 9$ angular points were used in the fiber-bundle domain, reflecting roughly the geometric aspect ratio of the HFBR cartridge studied here. The number of radial grid points within each ECS manifold (N_m) was found to have a negligible effect on the results ($< 0.1\%$ for $N_m = 1$ vs. $N_m = 10$) and was set to 1. The time step Δt was chosen to be 10 s for all simulations, which ensured both satisfactory mass balances of the solutions and acceptable duration of each computational run. The protein distribution was assumed to have reached steady state as soon as the maximum local magnitude of dC/dt dropped below 10^{-5} kg m^{-3} s^{-1}. Note that a local criterion (based on the maximum $|dC/dt|$) was chosen rather than a global one (based on the average $|dC/dt|$) to account for possible significant local changes in concentration, confined to a small portion of the ECS (such as a result of significant downstream polarization or exchange of the protein between the fiber bundle and the manifolds).

The ECS heterogeneity index (*HetIx*) is introduced here as a parameter that conveniently quantifies the nonuniformity of solute distribution in the ECS. This issue is of primary importance in HFBR cell culture, where it is desired to minimize spatial heterogeneities of growth factors and nutrients. The following definition of *HetIx* was adopted

$$HetIx = \frac{\sum_i |C_i - C_B| V_{i,ECS}}{2 C_B V_{ECS}} \tag{19}$$

where the summation is taken over all grid points; C_i is the local ECS solute (protein) concentration; $C_B = \Sigma_i\ C_i V_{i,\mathrm{ECS}} / V_{\mathrm{ECS}}$ is the average bundle concentration; $V_{i,\mathrm{ECS}}$ is the ECS part of the ith control volume; and V_{ECS} is the total ECS volume excluding manifolds. The heterogeneity index defined in this way can vary between 0, corresponding to a perfectly uniform concentration field, and an upper limit, corresponding to a distribution in which all of the ECS solute (protein) is confined to the smallest control volume. This upper limit of *HetIx* quickly approaches 1 as the grid is refined and equals 0.999989 for the $50 \times 10 \times 9$ cylindrical grid used here.

Experimental

The experimental studies conducted herein had as their primary objective the qualitative validation of the present model and were mainly focused on visual observation using tracer protein solutions. The difficulties associated with the use of invasive methods such as the freeze-and-thaw technique (Piret and Cooney, 1990) in the quantitative determination of 3-D protein distributions in hollow-fiber cartridges include: (1) instability of some distributions upon the stoppage of ICS flow, especially in upward-flow cartridges; (2) large numbers of cartridge sections that are needed for a 3-D analysis; and (3) a limit of one data set per experiment, which poses a constraint on the collection of transient data and requires that the cartridges be readily available at low cost. Noninvasive methods, on the other hand, are much more expensive and may require some specific technical problems to be addressed. For example, the size of the magnet bore may limit the use of magnetic resonance imaging (MRI) in the studies of different HFBR orientations.

The experiments were performed using a Cuprophan membrane GFE-15 hollow-fiber cartridge (Gambro Dialysatoren, Hechingen, Germany) and solutions of azoalbumin (Sigma, St. Louis, MO) as a tracer protein. The redistribution throughout the ECS of this red-colored albumin derivative was observed through the transparent walls of the cartridge. The physical properties of azoalbumin (except its color) were assumed to be essentially the same as those for BSA. Before the experiments, the hollow-fiber membranes were thoroughly rinsed using a mixture of phosphate-buffered saline (PBS) and distilled water, according to the protocol described elsewhere (Łabęcki et al., 1998). After the rinsing and overnight equilibration of the membranes, the fluid was drained from the cartridge and the ICS was filled with PBS containing 0.1% NaN_3 (Baker, Phillipsburg, NJ) to inhibit bacterial growth. Next, the ICS ports were closed, and a solution of azoalbumin in PBS (also with 0.1% NaN_3) was recirculated through the ECS at 1.7–3.3 cm^3/s (100–200 mL/min) for 15–20 min using a peristaltic pump (Cole-Parmer, Barrington, IL), to start from a homogeneous distribution of the protein in that space. After the cartridge orientation was adjusted to the desired angle, a sample was taken to determine the initial ECS concentration, and the ECS ports were clamped. The ICS fluid recirculation at a desired flow rate was then started using another peristaltic pump (Cole-Parmer), which marked the onset of the experiment ($t = 0$).

Five different cartridge orientations were investigated: vertical with downward ICS flow ($\Psi = 0°$), inclined with downward ICS flow ($\Psi = 45°$), horizontal ($\Psi = 90°$), inclined with upward ICS flow ($\Psi = 135°$), and vertical with upward ICS flow ($\Psi = 180°$). The initial protein concentrations in the ECS were uniform and ranged from 4.09 to 6.16 kg/m^3, which are realistic levels for proteins in serum-containing media used for mammalian cell culture. The ICS flow rate was set to 14.2 cm^3/s (850 mL/min), a value higher than that normally used in cell culture but chosen here purposefully to amplify the magnitude of convective protein transport. A typical experiment was carried out until no further changes in the protein distribution were noticeable (that is, for about 6 h at $\Psi \leq 90°$, for 9 h at $\Psi = 135°$, and for 32 h at $\Psi = 180°$), which approximately marked a steady state. Additional experiments were also performed to confirm that the expected steady-state protein distributions could also be obtained when starting from a highly nonuniform initial ECS concentration field. All experiments were conducted at room temperature, $T = 296 \pm 2$ K (23 ± 2°C).

In the course of each experiment, photographs of the side view of the cartridge were taken periodically. The protein distribution captured in each picture was, in fact, a superposition of the concentration distributions in the vertical sections perpendicular to the direction of viewing throughout the cartridge thickness. A small quantity of azoalbumin was usually present in the ICS recycle fluid in each experiment as a result of transmembrane leakage. This phenomenon, monitored by ICS sampling, was not sufficiently significant to influence the

appearance of the protein distributions, although it did slightly reduce the ECS–ICS contrast in the photographs. Overall, the photographic images obtained were sufficiently informative for the purpose of a qualitative analysis.

Between the experiments, the ECS contents were homogenized by fluid recirculation, and an ECS sample was taken to determine its protein concentration. The azoalbumin samples were assayed by spectrophotometric analysis using a Spectronic 601 device (Milton Roy, Rochester, NY) and absorbance measurements at 450 nm (characteristic absorption of the azo group). Additional measurements were also carried out at 280 nm (absorption of aromatic rings in the polypeptide chain) to confirm that the observed color intensity was indeed representative of the protein concentration.

ECS azoalbumin transport experiments similar to those described above were also carried out using a GFS Plus 16 Hemophan membrane dialyzer (Gambro). The trends of protein redistribution in the GFS Plus 16 reactor were generally less pronounced because of the reduced convective polarization and longer transients involved, which could be attributed to the differences in geometry and membrane permeability for the two HFBRs. The results of these latter studies (not shown) do not differ qualitatively from those obtained for the GFE-15 cartridge.

Results and Discussion

Preliminary simulations

Preliminary simulations showed that the predicted protein concentrations were virtually unaffected by the replacement of the inhomogeneous continuity Eq. 4a with its homogeneous form, Eq. 4b. Because poorer mass balances of the fluid were obtained with Eq. 4a, all subsequent simulations were performed using the homogeneous Eq. 4b. Likewise, viscosity gradients were found to have virtually no effect on the protein distribution but an adverse effect on fluid mass balance, and were therefore neglected. In both of these cases, the deterioration of the fluid mass balance was caused by the presence of additional gradient terms, which were evaluated by linear interpolation of the density and viscosity profiles from the centers to the faces of the control volumes (that is, from concentration grid points to velocity grid points).

Experimental validation of the model

Figure 2 compares experimental (top photos) and model-simulated (middle panels) ECS azoalbumin distributions at three different HFBR cartridge orientations after 6 h of closed-shell ICS fluid recirculation. The corresponding model-predicted ECS fluid velocities are plotted in the bottom panels of Figure 2. Additional experiments of longer duration have confirmed that the ECS protein distributions shown in Figure 2 are not significantly different from the steady-state ones (not shown). The model-predicted results (middle and bottom panels) are plotted in the longitudinal section through the cartridge centerline; this section was chosen as a sufficiently accurate representation of the depth-averaged distributions viewed from the side of the experimental cartridges (top photos). The small rectangles (not drawn to scale) outside the ECS domain in the graphs illustrating the model predictions indicate the axial positions of ECS manifolds. For simplicity, the manifold concentrations are not shown but are essentially the same as in the adjacent ECS fiber bundle at the respective axial positions.

For the benefit of visual comparison, the hue and intensity of the color in the predicted protein concentration plots (Figure 2, middle panels) were adjusted so as to best reproduce the appearance of the azoalbumin-filled experimental cartridges in the photographs (Figure 2, top panels). This was sufficient for the purpose of qualitative model validation. As Figure 2 demonstrates, using three sample HFBR orientations, the model-simulated protein distributions near steady state ($t = 6$ h) agreed well with experimental observations. It should be pointed out that similarly good agreement was obtained for transient distributions (results not shown; see Łabęcki, 2001). The apparent underestimation by the model of the concentrations in the manifolds can be explained partly by a larger fluid thickness in these regions and partly by the simplified way in which the manifold concentrations were calculated. Nevertheless, the essential features of the protein distribution within the ECS fiber bundle (such as the top-to-bottom concentration gradient at $\Psi = 135°$) were correctly captured by the model. More detailed quantitative comparisons were not possible because of experimental limitations in obtaining 3-D ECS concentration data at different time points.

Free-convective effects

As is evident from the bottom panel of Figure 2A, there was practically no free convection in the downward-flow cartridge ($\Psi = 45°$), and the observed ECS fluid movement was mainly the result of ICS flow and transmembrane fluid passage. In the horizontal case ($\Psi = 90°$), a free-convective recirculation loop developed downstream within a few hours, coinciding in space with the high-concentration protein region. As the inclination angle was increased to 135°, the gravitational contribution also increased, and the free-convective loop extended to the entire ECS. The significant convective flows present in the horizontal and upward-flow cartridges persisted even after steady state was reached, maintaining a dynamic balance of the local influx and outflow of protein at every point of the ECS. Unlike in the downward-flow case ($\Psi = 45°$), where osmotic effects effectively shut down hydrodynamics in the downstream-polarization zone (Łabęcki et al., 1996; Taylor et al., 1994), neither ECS flow nor transmembrane fluid exchange was diminished in the protein-rich region at $\Psi \geq 90°$.

The mechanism of ECS protein redistribution in the presence of significant free convection can be elucidated by discussing the model-predicted transients for $\Psi = 135°$ (Figure 3). This inclined orientation with upward ICS flow is commonly used in commercial cell culture HFBR systems because it has been observed to provide a relatively homogeneous growth environment. As is illustrated in Figure 3, the first hour of ICS fluid recirculation causes forced-convective downstream polarization of the protein. This process is to some extent delayed by protein exchange with the ECS manifolds, creating a positive radial concentration gradient at the upstream end and a negative radial gradient at the downstream end. A characteristic free-convective swirl develops in the region of protein accumulation, pulling the concentrated solution toward the bottom of the cartridge ($t = 1.5$ h) and then upstream ($t = 2$ h). As the bottom-polarized protein spreads over the entire length of the bioreactor, the upstream-moving fluid finds its way back down-

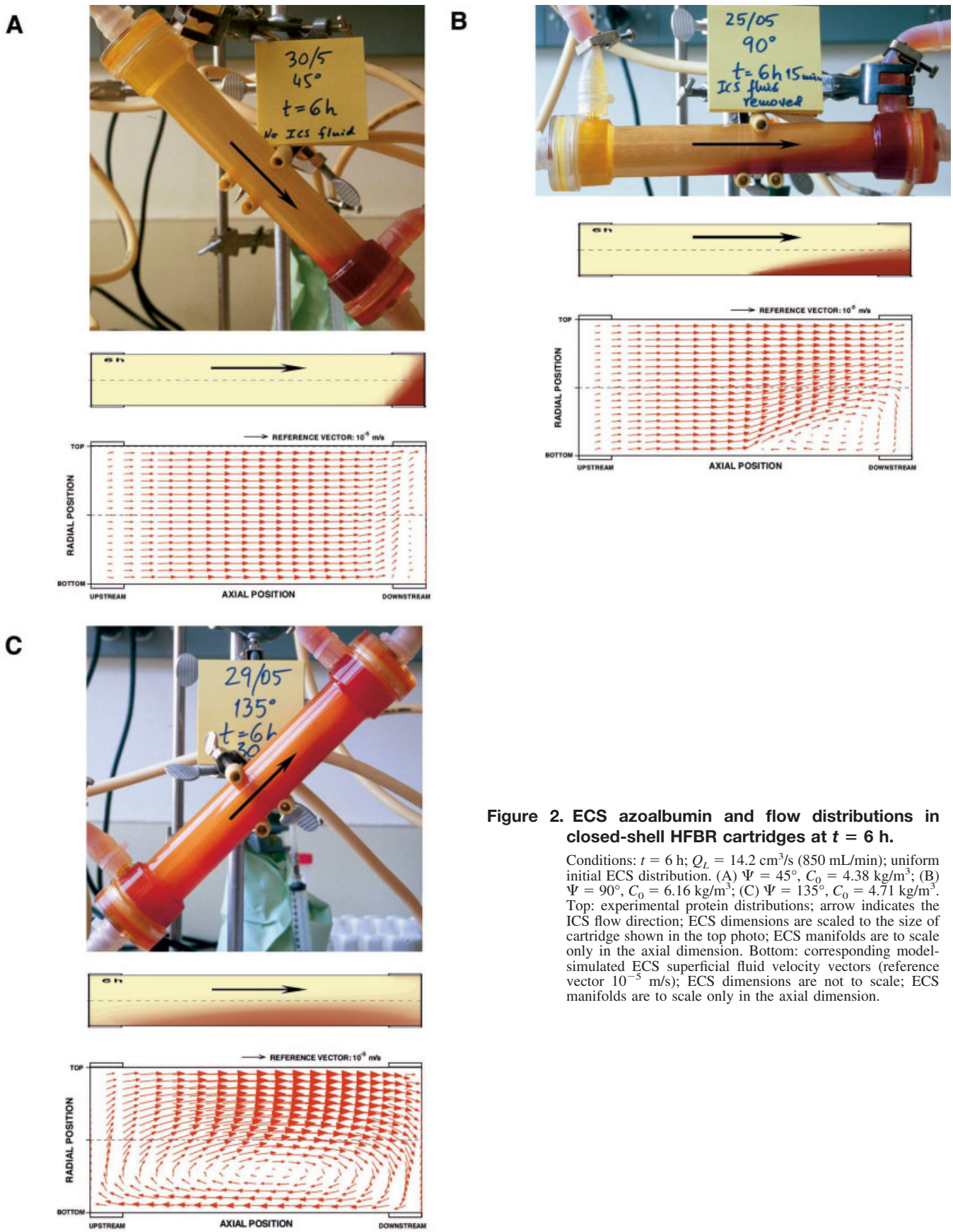

Figure 2. ECS azoalbumin and flow distributions in closed-shell HFBR cartridges at t = 6 h.

Conditions: t = 6 h; Q_L = 14.2 cm^3/s (850 mL/min); uniform initial ECS distribution. (A) Ψ = 45°, C_0 = 4.38 kg/m^3; (B) Ψ = 90°, C_0 = 6.16 kg/m^3; (C) Ψ = 135°, C_0 = 4.71 kg/m^3. Top: experimental protein distributions; arrow indicates the ICS flow direction; ECS dimensions are scaled to the size of cartridge shown in the top photo; ECS manifolds are to scale only in the axial dimension. Bottom: corresponding model-simulated ECS superficial fluid velocity vectors (reference vector 10^{-5} m/s); ECS dimensions are not to scale; ECS manifolds are to scale only in the axial dimension.

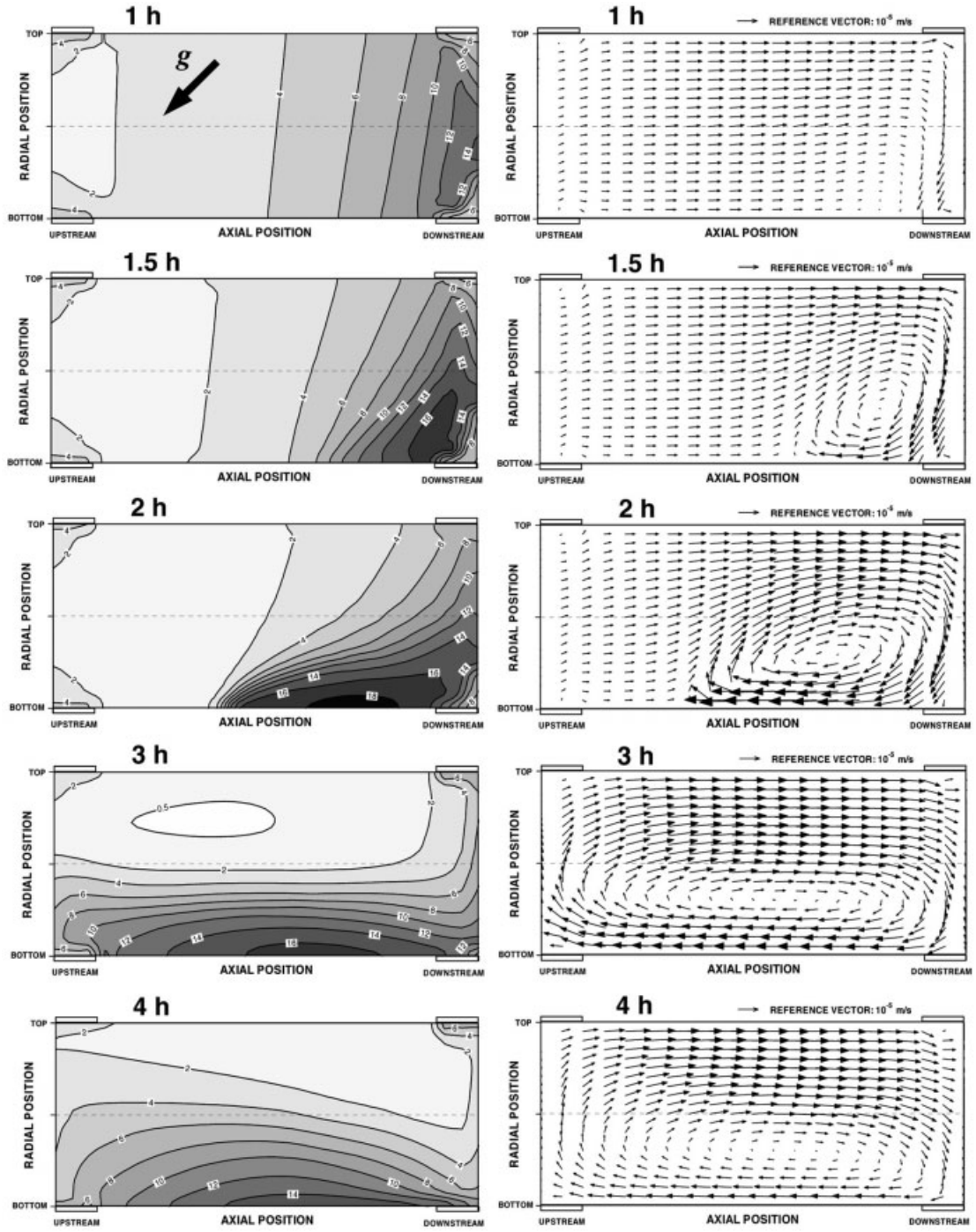

Figure 3. Model-predicted transients in the vertical section through the cartridge centerline for $\Psi = 135°$.

Left: ECS protein concentration contours (kg/m^3); right: ECS superficial fluid velocities (reference vector 10^{-5} m/s). ICS flow from left to right, $Q_L = 10$ cm^3/s (600 mL/min), $C_0 = 5$ kg/m^3. The direction of gravitational acceleration is shown in the top left panel.

stream through the upper portion of the ECS, where the concentration is lower ($t = 3$ h). Thus, the fluid recirculation loop is closed, encompassing now the whole ECS and carrying the protein along by convective motion. Later ($t \geq 4$ h), the concentration gradients and free-convective flows decrease as the system approaches its steady state (compare Figure 2C). After 4 h, no further significant changes occur to the ECS hydrodynamics or concentration distribution, with the protein spread mainly along the bottom of the cartridge.

The ECS protein redistribution in vertical cartridges with upward flow is even more strongly influenced by gravity and is thus more complex. To account for nonuniformities in fiber packing and other factors possibly disturbing the symmetry of nonideal hollow-fiber cartridges, the 1° off-vertical inclination

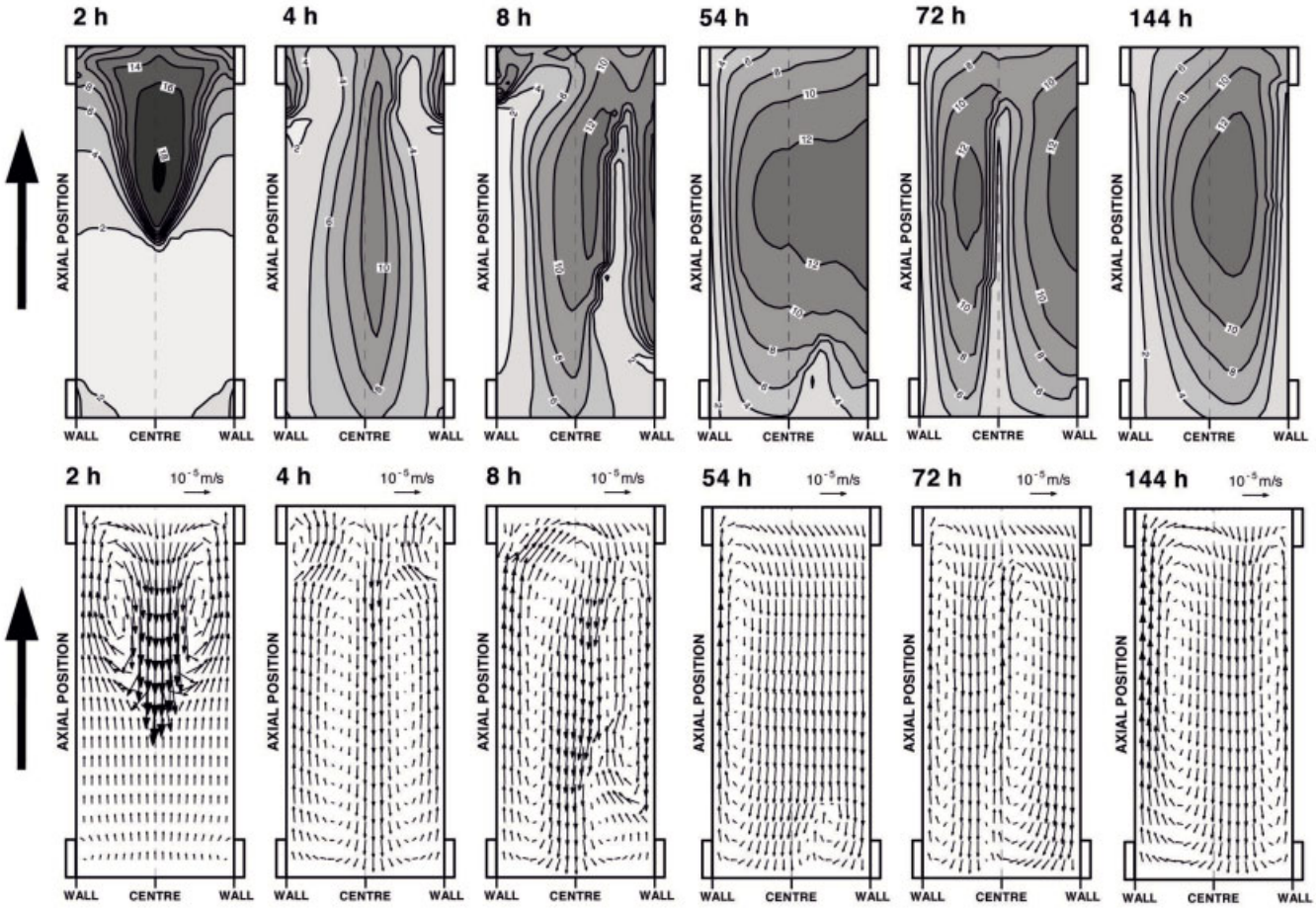

Figure 4. Model-predicted transients in the vertical section through the cartridge centerline for $\Psi = 179°$ (top of cartridge inclined 1° to the right).

Top row: ECS protein concentrations (kg/m^3); bottom row: ECS superficial fluid velocities. Upward ICS flow as indicated by arrows on the left; $Q_L = 10$ cm^3/s (600 mL/min), $C_0 = 5$ kg/m^3. ECS dimensions not to scale; ECS manifolds to scale only in the axial dimension.

($\Psi = 179°$) was chosen as a more realistic representation of this case than the perfectly axisymmetric orientation of $\Psi = 180°$. Because of strong nonlinearities associated with gravitational influences, the hydrodynamics and protein transport at these orientations are very sensitive to small perturbations such as an off-vertical tilting. Note that the symmetry also changes from axial to planar when the ICS flow is directed down and Ψ is changed from 0 to 1°. In the latter case, however, because of the relative insignificance of the gravitational contribution, the system's response to such a perturbation is linear, that is, with infinitesimally small changes to its properties.

Selected ECS transients for 179° are shown in Figure 4. During the initial 2 h, the 1° off-vertical cartridge tilting has virtually no effect on the results, and the protein concentration and fluid velocity distributions are practically axisymmetric. As the protein is polarized downstream by forced convection, the upward gradient of fluid density increases, and the resulting free-convective flows spread the protein downward ($t = 2$ h). The flow perturbation attributed to cartridge tilting continues to grow ($t = 4$ h), and the system eventually loses its axial symmetry ($t \approx 8$ h). Later ($t \geq 8$ h), numerous transient convective loops develop in regions of high upward concentration gradients, facilitating mixing in the ECS. For example, a major clockwise convective loop is seen at $t = 54$ h, with the protein spread throughout the ECS but polarized in the direction of cartridge tilting, that is, toward the right-hand-side wall (Figure 4). This distribution is unstable, which can be seen from the formation of a small clockwise loop near the bottom end of the ECS ($t = 54$ h). Within the subsequent 18 h or so, this minor loop stimulates its own growth by recirculating the protein upward toward the high-concentration zone, which increases the local concentration gradient and hence also the magnitude of free-convective transport ($t = 72$ h). Similar flow and concentration fields periodically arise and disappear several times before steady state is reached, with the final distributions virtually identical to those shown for $t = 144$ h.

Because of the imposed axial symmetry and the absence of angular gradients, the dynamics of a perfectly vertical system (results not shown) are more "stiff" and less complex than those described above for $\Psi = 179°$. For example, the onset of free-convective downward protein redistribution at $\Psi = 180°$ is predicted to occur about 30–45 min later than in the off-vertical case. Furthermore, sideways-polarized concentration fields such as that of $t = 54$ h at $\Psi = 179°$ (Figure 4) cannot arise at $\Psi = 180°$, and both the transient (after the initial polarization period) and steady-state distributions are generally

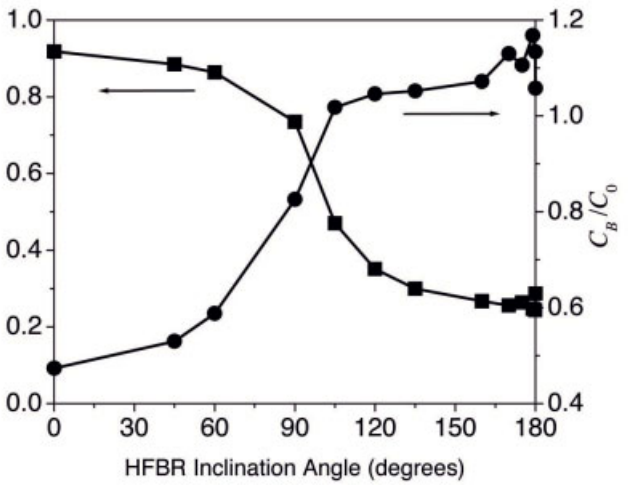

Figure 5. Steady-state output parameters as functions of the HFBR inclination angle.

Left axis, squares: ECS heterogeneity index (*HetIx*); right axis, circles: average dimensionless ECS fiber bundle concentration (C_B/C_0); $C_0 = 5$ kg/m^3, $Q_L = 10$ cm^3/s (600 mL/min). The shapes of the curves are virtually unchanged if *HetIx* and C_B/C_0 are plotted at a sufficiently long time (such as $t = 24$ h) rather than at steady state. Note the highly nonlinear behavior reflected in the fluctuations of both curves at $\Psi > 170°$.

different for these two inclination angles. Despite their differences, the vertical and off-vertical upward-flow HFBR orientations are similar in terms of the existence of strong free-convective flows that very effectively mix the ECS contents, thus creating favorable conditions for cell culture.

Effect of cartridge inclination angle

The HFBR orientation has a strong effect on ECS protein distribution, with an increasing role of free-convective transport as the direction of ICS flow changes from vertical-down ($\Psi = 0°$) to horizontal ($\Psi = 90°$) and vertical-up ($\Psi \approx 180°$). This has important practical implications, given that the heterogeneity of ECS growth-factor distribution can seriously impair cell growth and overall culture productivity. The data presented above strongly indicate that upward ICS flow configurations ($\Psi > 90°$), where the free-convective mixing of the ECS fluid is most effective, are the best options for HFBR operation. In particular, the vertical-upflow configuration ($\Psi \approx 180°$)—currently uncommon in HFBR cell culture applications—seems quite promising, as long as cell sedimentation is not excessive.

The steady-state ECS protein heterogeneity index (*HetIx*) and the average ECS protein concentration in the fiber bundle (C_B), predicted for different HFBR inclination angles, are plotted in Figure 5. Both of these parameters are important in cell culture. Heterogeneous distribution of ECS growth factors may lead to nonuniform cell growth and inefficient use of HFBR space, whereas a decrease in C_B below the input level indicates the possibility of growth factor depletion resulting from accumulation in the ECS manifolds. Figure 5 strongly emphasizes the difference between downward- and upward-flow orientations, given that the S-shaped profiles of *HetIx* and C_B have their inflexion points near $\Psi = 90°$. It is clear that the only inclination angles of practical interest for HFBR cell culture are those of at least 100°.

At $\Psi = 170°$, interestingly, a periodic solution emerged after about 50 h, oscillating with a frequency of about 0.033 mHz (period 8.5 h). It is not clear whether this periodicity reflected an intrinsic property of the differential equation system or was merely a numerical artifact, although periodic solutions at $\Psi = 170°$ also arose when the spatial grid was refined. At near-vertical orientations ($\Psi > 170°$), nonperiodic solutions were obtained, but the results were increasingly nonlinear and very sensitive to Ψ, as is reflected by the fluctuations of both curves in Figure 5. Overall, however, the steady-state *HetIx* was lowest and C_B highest at $\Psi \approx 180°$, which strengthens the proposition that the vertical or near-vertical orientation with upward flow might successfully compete with the standard HFBR inclination angle of 135°.

In situations where an overall assessment of the ECS state at a given time is needed, a plot of *HetIx* vs. time may be preferred to the fluid velocity vector and protein concentration contour graphs shown in Figures 2–4. Figure 6 presents the temporal *HetIx* profiles for selected cartridge orientations at the initial ECS protein level $C_0 = 5$ kg/m^3 (uniform) and the ICS flow rate $Q_L = 10$ cm^3/s (600 mL/min). As can be seen, all of the curves level off within about 15 h. For the horizontal and downward-flow cartridges, the profiles rise monotonically and reach plateau values exceeding 0.7. As the cartridge orientation changes from horizontal to vertical-upflow, the plateau values decrease to less than 0.3, and damped oscillations of *HetIx* become increasingly noticeable, reflecting the alternation of forced-convective protein polarization and free-convective protein redistribution. Temporal plots of *HetIx* for growth-factor or product proteins for different combinations of operating conditions could be helpful in planning and optimizing HFBR operation.

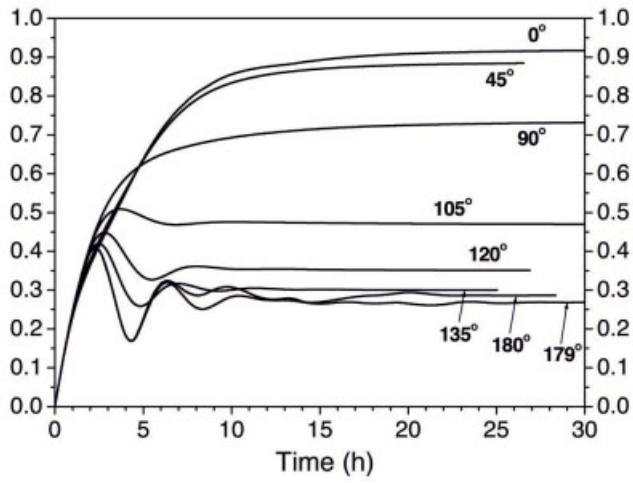

Figure 6. Model-predicted temporal changes of the ECS protein heterogeneity index (*HetIx*) for different orientations of the HFBR cartridge.

Uniform initial concentration field, $C_0 = 5$ kg/m^3, $Q_L = 10$ cm^3/s (600 mL/min); other input parameters are at their default values.

Table 2. Model-Predicted Effects of Manifold Size on the ECS Protein Heterogeneity Index (*HetIx*) and the Average Protein Concentration in the Fiber Bundle (C_B) at Steady State for Different Cartridge Orientations*

	Change in Steady-State *HetIx* Due to ECS Manifolds		Change in Steady-State C_B Due to ECS Manifolds	
Cartridge Orientation	Normal Manifolds	Double-Size Manifolds	Normal Manifolds	Double-Size Manifolds
0° (vertical down)	+0.076	+0.091	−53%	−64%
45° (inclined down)	+0.059	+0.075	−47%	−62%
90° (horizontal)	+0.036	+0.059	−17%	−28%
135° (inclined up)	−0.007	−0.011	+5%	+8%
179° (near-vertical up)	−0.022	−0.033	+17%	+28%
180° (vertical up)	−0.004	−0.045	+6%	+20%

*C_0 = 5 kg/m^3, Q_L = 10 cm^3/s (600 mL/min). The listed values represent absolute (*HetIx*) or percentage (C_B) changes, relative to a hypothetical cartridge with no ECS manifolds. Note the trend deviation resulting from a change in symmetry at Ψ = 180°.

Effect of ECS manifolds

To investigate the effect of ECS manifolds, two additional cases were simulated: (1) a hypothetical cartridge with no manifolds and (2) a hypothetical cartridge with manifolds of twice the normal size. From the perspective of cell culture, the most important aspect of the manifolds' involvement is their entrapment of proteins (as well as cells), which can adversely affect both the average level of growth factors in the ECS fiber bundle and the heterogeneity of their distribution. Table 2 illustrates these effects by listing the changes in the steady-state *HetIx* and C_B resulting from the addition of normal and double-size manifolds to a hypothetical, manifold-free cartridge. For growth-factor proteins, *HetIx* should ideally be low and C_B high, and the desired changes in *HetIx* and in C_B attributed to manifold addition should be negative and positive, respectively.

By and large, the manifolds were responsible for increases in *HetIx* and decreases in C_B in horizontal and downward-flow cartridges, whereas the opposite trends were observed for upward-flow cartridges (Table 2). The trend deviation observed at $\Psi \approx 180°$ was ascribed to a change in symmetry and the absence of angular gradients, as explained above. The results presented in Table 2 clearly indicate that HFBR inclination angles $\Psi \geq 135°$ should be used to avoid the adverse effects of the manifolds. Moreover, it appears that larger manifolds would have a greater advantage to cell culture at these reactor orientations, at least from the perspective of growth-factor distribution. However, the predicted effects of the manifold size are not linear, because the manifold volume in the simulations was varied without changing the surface area of the manifold–bundle boundary. The role of the ECS manifolds will also become apparent in the discussions of the effects of C_0 and Q_L (see below).

Effects of ECS protein content and ICS flow rate

The ECS protein distribution can be expected to become more homogeneous if the ECS is loaded with more protein, that is, if C_0 is increased to a sufficiently high level. This is because, under convection-dominated transport conditions, there exists a maximum level of local protein concentration, determined by the distributions of hydrostatic and osmotic pressures on both sides of the membrane (Patkar et al., 1995; Taylor et al., 1994); addition of protein above that level causes it to spread over a larger part of the ECS (depending also on HFBR orientation). Note that at low HFBR protein loadings, as well as during transients, free convection probably plays a more significant role in homogenizing the protein content than do the osmotic effects. The C_0 value of 5 kg/m^3, used in most simulations discussed above, represents a realistic concentration level for serum-supplemented HFBR cell culture. This section will briefly discuss two cases investigated using different C_0 values (at Q_L = 10 cm^3/s). In one case, the initial concentration was increased to 20 kg/m^3, roughly the upper limit of what can be reasonably expected for a serum-supplemented ECS culture medium. In the other case, C_0 was reduced to 1 kg/m^3, which is more representative of serum-free media supplemented with growth factor proteins.

The effects of the simulated changes in C_0 on the protein distribution heterogeneity and the average protein concentration in the fiber bundle at steady state are illustrated in Figure 7. As can be seen, the fourfold increase in C_0 to 20 kg caused an approximately twofold reduction of *HetIx* at all inclination angles (Figure 7, top panel). For upward-flow orientations, the heterogeneity index was approximately doubled as a result of a fivefold decrease in C_0 to 1 kg/m^3. At $\Psi \leq 90°$, the increases in *HetIx* were much less pronounced because the index was

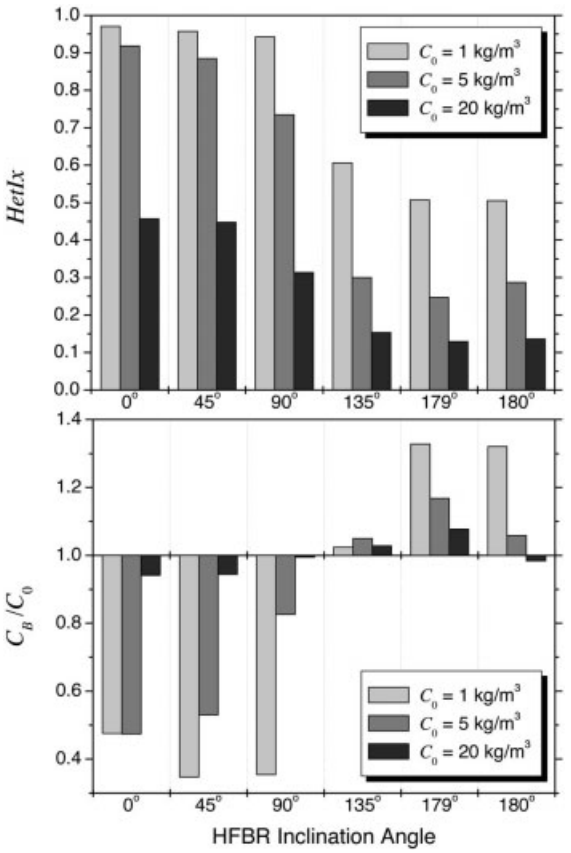

Figure 7. Effects of the initial ECS protein concentration (C_0) and the HFBR inclination angle on the ECS heterogeneity index (top) and the ECS fiber bundle concentration (bottom) at steady state.

Q_L = 10 cm^3/s, normal manifolds.

Table 3. Effects of a Threefold Reduction in Q_L on the ECS Heterogeneity Index (*HetIx*) and the Fiber Bundle Concentration (C_B/C_0) at Steady State*

	HetIx		C_B/C_0	
Cartridge Orientation	10 cm^3/s	3.3 cm^3/s	10 cm^3/s	3.3 cm^3/s
0° (vertical down)	0.92	0.72	0.47	0.77
45° (inclined down)	0.89	0.70	0.53	0.78
90° (horizontal)	0.73	0.43	0.83	0.97
135° (inclined up)	0.30	0.17	1.05	1.02
179° (near-vertical up)	0.25	0.15	1.17	1.07
180° (vertical up)	0.29	0.15	1.06	0.99

*C_0 = 5 kg/m^3, normal manifolds.

already close to its maximum level at $C_0 = 5$ kg/m^3. At $C_0 = 1$ kg/m^3, the predicted steady-state *HetIx* values remained above 0.5 even at the highest inclination angles.

At the highest protein loading (20 kg/m^3), the deviation of C_B from C_0 is reduced to less than 8% (Figure 7, bottom panel), clearly indicating a diminished role of the ECS manifolds. Conversely, a significant impact of the manifolds on C_B is evident at $C_0 = 1$ kg/m^3. In this case, the model predicts over 30% enrichment of the fiber bundle with protein released from the manifolds at $\Psi \approx 180°$, and over 50% depletion in protein as a result of manifold entrapment at $\Psi \leq 90°$. Interestingly, the steady-state C_B/C_0 ratio at $\Psi = 135°$ is almost unaffected by the initial protein concentration and remains close to 1. The decline in C_B with Ψ increasing from 0 to 45° at $C_0 = 1$ kg/m^3 is somewhat unexpected and opposes the overall trend predicted for higher C_0. It can perhaps be attributed to more favorable conditions of protein transfer from the bundle to the downstream manifold at $\Psi = 45°$ than at $\Psi = 0°$, given that the surface area of the high-concentration protein zone boundary is larger in the former case. Such an anomaly could be observed only at sufficiently low protein loadings for a given manifold volume.

As expected, the heterogeneity of the ECS protein distribution can also be reduced by lowering the ICS flow rate. In this case, the trends of *HetIx* and C_B changes with Q_L for different HFBR orientations (Table 3) are qualitatively similar to those resulting from an increase in C_0. Thus, an adjustment of either C_0 or Q_L might be considered as a means of controlling the ECS protein heterogeneity in cell culture HFBRs at a given reactor orientation. For example, the ECS protein content could be easily increased by the addition of a relatively inexpensive medium protein such as BSA. In such a case, the distribution of growth factors would be expected to follow that of the excess protein (Patkar et al., 1995). This method of intervention may indeed be preferred over the manipulation of the ICS flow rate, which is constrained by the need to supply sufficient amounts of oxygen and nutrients to the bioreactor. However, consequences of protein addition to the efficiency of downstream product separation would have to be considered before such a measure is implemented in cell culture.

Conclusions

The subject of this study was the dynamics of ECS protein transport and fluid flow in closed-shell HFBRs under the influence of gravity. The ECS fluid density gradients associated with downstream-polarized protein concentration fields arising in closed-shell HFBRs can trigger a free-convective redistribution of the protein. A number of numerical simulations were carried out to determine how this process depended on the HFBR design parameters and operating conditions. Of particular interest were the effects of the cartridge inclination angle, total ECS protein loading, and the presence of ECS manifolds.

The three-dimensional porous medium model presented here accounts for spatial and temporal variations of ECS fluid density, fluid viscosity, and osmotic pressure, through their dependence on protein concentration. The effects of protein exchange between the ECS fiber bundle and fiber-free manifold regions were also included in a simplified fashion. The model was successfully validated in a qualitative sense by comparing the predicted protein concentration fields with experimental distributions of azoalbumin used as a tracer protein, both during transients and at steady state. A detailed quantitative validation proved much more difficult because of experimental limitations in obtaining transient 3-D protein distribution data, and to nonidealities existing in real HFBR cartridges, such as nonuniform fiber packing. Sufficient accuracy of numerical results was obtained by neglecting fluid viscosity gradients and by assuming a homogeneous form of the ECS fluid continuity equation.

The extent and magnitude of free convection in the ECS depends dramatically on the HFBR orientation [that is, the angle between the directions of bulk ICS flow and gravitational force (Ψ)]. In horizontal and downward-flow cartridges ($\Psi \leq 90°$), free-convective flows are limited in scope and, at typical protein loadings ($C_0 \approx 5$ kg/m^3), downstream-polarized protein distributions prevail at steady state. The resulting heterogeneity of the ECS culture environment can limit cell growth and bioreactor operation (Piret and Cooney, 1990). In inclined and vertical cartridges with upward ICS flow ($\Psi > 90°$), free-convective flows redistribute the protein over the ECS volume, thus creating more homogeneous and hence more favorable conditions for cell growth. The vertical-upflow HFBR orientation ($\Psi \approx 180°$), currently nonstandard, seems very promising for cell culture because of particularly effective free-convective mixing in the ECS. Additional studies are needed to verify the feasibility of this configuration with respect to cell distribution in the ECS.

The ECS manifolds were found to accelerate the development of free-convective instabilities and transient recirculatory flows in the ECS, particularly at $\Psi \approx 180°$. Larger manifolds were predicted to make the ECS protein distribution less heterogeneous at $\Psi > 90°$, and more heterogeneous at $\Psi \leq 90°$. A net protein release from the manifolds to the fiber bundle should generally occur at $\Psi > 90°$, whereas decreases in the bundle concentration below its initial level were predicted for $\Psi \leq 90°$, attributed to protein accumulation in the manifolds. In addition to choosing an upward-flow HFBR configuration, the heterogeneity of protein distribution in the ECS could be further reduced by increasing the protein loading or by lowering the ICS flow rate.

The above results have important implications to the HFBR operation. Because the cells can grow only in close proximity to a source of oxygen, that is, within the fiber bundle, a possible depletion of ECS growth-factor proteins resulting from their entrapment in the manifolds creates a serious risk of culture failure in horizontal and downward-flow cartridges. This is particularly important at low growth-factor concentrations ($C_0 < 1$ kg/m^3) typical of serum-free culture media. Supplemen-

tation of the ECS medium with a large quantity of an inert protein such as albumin could be one way of alleviating this problem.

From the perspective of minimizing the cost of downstream processing, protein accumulation in the downstream manifold, near the ECS outlet port, may be used to increase the product concentration in the harvest. ECS protein transfer from the bundle to the manifolds may also be beneficial to the culture in the case of a product that inhibits its own secretion (Dowd et al., 2000). These potential advantages, however, should be carefully weighed against the definite disadvantages of entrapment of cells and growth factors inside the ECS manifolds.

Acknowledgments

Natural Sciences and Engineering Research Council of Canada (NSERC) has provided financial support for this project.

Notation

A_{F1}, A_{F12} = coefficients defined by Eqs. A10 and A11, respectively
A_L, A_S = right-hand-side coefficients defined by Eqs. A9 and A7, respectively, Pa
A_{L2} = coefficient in Eq. 11, defined by Eq. A8, m^2
A_{Lp} = coefficient defined by Eq. A12, Pa s^{-1}
$A_{r1}, A_{\theta 1}, A_{z1}$ = coefficients defined by Eqs. A4, A5, and A6, respectively, m
$A_{r2}, A_{\theta 2}, A_{z2}$ = coefficients defined by Eqs. A1, A2, and A3, respectively, m^2
$A_{\mu 1}, A_{\Pi 1}$ = virial coefficients in Eqs. 15 and 17, respectively, m^3 kg^{-1}
$A_{\mu 2}, A_{\Pi 2}$ = virial coefficients in Eqs. 15 and 17, respectively, m^6 kg^{-2}
A_V = membrane surface area per unit volume available for fluid transport, m^{-1}
C = ECS protein concentration, kg m^{-3}
C_B = average protein concentration in the ECS fiber bundle, kg m^{-3}
C_i = protein concentration in the ith control volume of the ECS, kg m^{-3}
D = free-fluid protein diffusivity, m^2 s^{-1}
D_A = free-fluid BSA diffusivity at $T = 293$ K, m^2 s^{-1}
F_1 = on/off switch for inhomogeneous fluid continuity terms in Eq. A13
F_μ = on/off switch for ECS fluid viscosity gradients in Eqs. A4–A7
g = gravitational acceleration, 9.81 m s^{-2}
h = elevation above datum level, m
$HetIx$ = heterogeneity index (Eq. 19)
J_P = protein flux, kg m^{-2} s^{-1}
J_{TMF} = transmembrane fluid flux, m s^{-1}
J_{TMP} = transmembrane protein flux, kg m^{-2} s^{-1}
k = Darcy hydraulic permeability, m^2
L = length of the ECS domain, m
L_p = membrane hydraulic permeability, m
M = molar mass, kg mol^{-1}
n = number of fibers in the HFBR cartridge
N_i, N_j, N_k = numbers of grid points in the axial, radial, and angular dimensions, respectively
N_m = number of radial grid points within the ECS manifold
P = hydrostatic pressure, Pa
$\hat{P}$ = piezometric pressure ($=P + \rho_0 gh$), Pa
Q_L = ICS flow rate, cm^3 s^{-1}
r = radial position, m
R_{HFBR} = hollow-fiber cartridge radius, m
R_g = universal gas constant, 8.314 J mol^{-1} K^{-1}
R_F = fiber outer radius, m
R_L = fiber lumen radius, m
Re = Reynolds number
t = time, s
T = temperature, K
v = superficial fluid velocity, m s^{-1}
V_{ECS} = ECS volume excluding manifolds, cm^3
V_m = volume of each ECS manifold, cm^3
x_i = general spatial variable (r, θ, or z)
z = axial position, m
z_m = axial length of the ECS manifold, m

Greek letters

Δt = time step, s
Δz = axial grid increment, m
$\Delta\Pi_{eff}$ = effective osmotic pressure difference, Pa
$\Delta\rho$ = reduced fluid density ($=\rho - \rho_0$), kg m^{-3}
$\Delta\rho'$ = dimensionless reduced fluid density ($=\rho/\rho_0 - 1$)
ϵ_S = ECS porosity
μ = fluid viscosity, Pa s^{-1}
Π = osmotic pressure, Pa
θ = angular position, °
ρ = fluid density, kg m^{-3}
ρ' = dimensionless fluid density ($=\rho/\rho_0$)
Ψ = cartridge inclination angle, °

Subscripts

0 = initial; protein-free solute
in = inlet
L = ICS (lumen side)
m = manifold
out = outlet
P = protein
r = radial
S = ECS (shell side)
z = axial
θ = angular

Abbreviations

3-D = three-dimensional
ADI = alternate direction implicit
BSA = bovine serum albumin
CV = control volume
ECS = extracapillary space (shell side)
HFBR = hollow-fiber bioreactor
ICS = intracapillary space (lumen side)
KCM = Krogh cylinder model
MAb = monoclonal antibody
MM = molar mass
MMCO = molar mass cutoff
PBS = phosphate-buffered saline
PMM = porous medium model

Literature Cited

Allen, J. W., T. Hassanein, and S. N. Bhatia. "Advances in Bioartificial Liver Devices," *Hepatology*, **34**, 447 (2001).

Anderson, J. L., F. Rauh, and A. Morales, "Particle Diffusion as a Function of Concentration and Ionic Strength," *J. Phys. Chem.*, **82**, 608 (1978).

Bear, J., *Dynamics of Fluids in Porous Media*, Dover Publications, New York (1972).

Douglas, J., "Alternating Direction Methods for Three Space Variables," *Numer. Math.*, **4**, 41 (1962).

Dowd, J. E., K. E. Kwok, and J. M. Piret, "Increased t-PA Yields Using Ultrafiltration of an Inhibitory Product from CHO Fed-Batch Culture," *Biotechnol. Prog.*, **16**, 786 (2000).

Gramer, M. J., D. M. Poeschl, M. J. Conroy, and B. E. Hammer, "Effect of Harvesting Protocol on Performance of a Hollow Fiber Bioreactor," *Biotechnol. Bioeng.*, **65**, 334 (1999).

Happel, J., "Viscous Flow Relative to Arrays of Cylinders," *AIChE J.*, **5**, 174 (1959).

Jackson, L. R., L. J. Trudel, J. G. Fox, and N. S. Lipman, "Evaluation of Hollow Fiber Bioreactors as an Alternative to Murine Ascites Production for Small Scale Monoclonal Antibody Production," *J. Immunol. Methods*, **189**, 217 (1996).

Kim, S.-S., and D. O. Cooney, "An Improved Theoretical Model for Hollow-Fiber Enzyme Reactors," *Chem. Eng. Sci.*, **31**, 289 (1976).
Koska, J., B. D. Bowen, and J. M. Piret, "Protein Transport in Packed-Bed Ultrafiltration Hollow-Fibre Bioreactors," *Chem. Eng. Sci.*, **52**, 2251 (1997).
Krogh, A., "The Number and Distribution of Capillaries in Muscles with Calculations of the Oxygen Pressure Head Necessary for Supplying the Tissue," *J. Physiol.*, **52**, 409 (1919).
Łabęcki, M., "Experimental and Theoretical Studies of Protein Transport in Hollow-Fibre Bioreactors for Mammalian Cell Culture," PhD Thesis, University of British Columbia, Canada (2001).
Łabęcki, M., B. D. Bowen, and J. M. Piret, "Two-Dimensional Analysis of Protein Transport in the Extracapillary Space of Hollow-Fibre Bioreactors," *Chem. Eng. Sci.*, **51**, 4197 (1996).
Łabęcki, M., B. D. Bowen, and J. M. Piret, "Protein Transport in Ultrafiltration Hollow-Fiber Bioreactors for Mammalian Cell Culture," *Membrane Separations in Biotechnology*, 2nd Edition, W. K. Wang, ed., Marcel Dekker, New York, pp. 1–62 (2001).
Łabęcki, M., J. M. Piret, and B. D. Bowen, "Two-Dimensional Analysis of Fluid Flow in Hollow-Fibre Modules," *Chem. Eng. Sci.*, **50**, 3369 (1995).
Łabęcki, M., I. Weber, Y. Dudal, J. Koska, J. M. Piret, and B. D. Bowen, "Hindered Transmembrane Protein Transport in Hollow-Fibre Devices," *J. Membr. Sci.*, **146**, 197 (1998).
Lee, Y.-T., O. Henry, H. A. L. Sczerba, B. D. Bowen, and J. M. Piret, "Factors Affecting Hybridoma Cell Growth during Start-Up of Hollow Fibre Bioreactor," *Biotechnol. Bioeng.*, (Submitted 2003).
Malone, C. C., P. M. Schiltz, A. D. Mackintosh, L. D. Beutel, F. S. Heinemann, and R. O. Dillman, "Characterization of Human Tumor-Infiltrating Lymphocytes Expanded in Hollow-Fiber Bioreactors for Immunotherapy of Cancer," *Cancer Biother. Radiopharm.*, **16**, 381 (2001).
Patankar, S. V., *Numerical Heat Transfer and Fluid Flow*, Hemisphere, Washington, DC (1980).
Patkar, A. Y., J. Koska, D. G. Taylor, B. D. Bowen, and J. M. Piret, "Protein Transport in Ultrafiltration Hollow Fiber Bioreactors," *AIChE J.*, **41**, 415 (1995).
Perry, R. H., and D. Green, eds., *Perry's Chemical Engineering Handbook*, 6th Edition, McGraw-Hill, New York (1984).
Pillarella, M. R., and A. L. Zydney, "Theoretical Analysis of the Effect of Convective Flow on Solute Transport and Insulin Release in a Hollow Fiber Bioartificial Pancreas," *J. Biomech. Eng.* (*Trans. ASME*), **112**, 220 (1990).
Piret, J. M., and C. L. Cooney, "Mammalian Cell and Protein Distributions in Ultrafiltration Hollow-Fiber Bioreactors," *Biotechnol. Bioeng.*, **36**, 902 (1990).
Piret, J. M., and C. L. Cooney, "Model of Oxygen Transport Limitations in Hollow Fiber Bioreactors," *Biotechnol. Bioeng.*, **37**, 80 (1991).
Rony, P. R., "Multiphase Catalysis. II. Hollow-Fiber Catalysts," *Biotechnol. Bioeng.*, **13**, 431 (1971).
Salmon, P. M., S. B. Libicki, and C. R. Robertson, "A Theoretical Investigation of Convective Transport in the Hollow-Fiber Reactor," *Chem. Eng. Commun.*, **66**, 221 (1988).
Starling, E. H., "On the Absorption of Fluids from the Connective Tissue Spaces," *J. Physiol.*, **19**, 312 (1896).
Tannehill, J. C., D. A. Anderson, and R. H. Pletcher, *Computational Fluid Mechanics and Heat Transfer*, 2nd Edition, Taylor & Francis, Philadelphia (1997).
Taylor, D. G., J. M. Piret, and B. D. Bowen, "Protein Polarisation in Isotropic Membrane Hollow-Fiber Bioreactors," *AIChE J.*, **40**, 321 (1994).
Tharakan, J. P., S. Gallagher, and P. C. Chau, "Hollow Fiber Bioreactors in Mammalian Cell Culture," *Adv. Biotechnol. Process.*, **7**, 153 (1988).
van den Berg, G. B., and C. A. Smolders, "The Boundary-Layer Resistance Model for Unstirred Ultrafiltration. A New Approach," *J. Membr. Sci.*, **40**, 149 (1989).
Vilker, V. L., C. K. Colton, and K. A. Smith, "The Osmotic Pressure of Concentrated Protein Solutions: Effect of Concentration and pH in Saline Solutions of Bovine Serum Albumin," *J. Colloid Interface Sci.*, **79**, 548 (1981).
Waterland, L. R., A. S. Michaels, and C. R. Robertson, "A Theoretical Model for Enzymatic Catalysis Using Asymmetric Hollow-Fiber Membranes," *AIChE J.*, **20**, 50 (1974).
Waterland, L. R., C. R. Robertson, and A. S. Michaels, "Enzymatic Catalysis Using Asymmetric Hollow Fiber Membranes," *Chem. Eng. Commun.*, **2**, 37 (1975).
Weast, R. C., ed., *Handbook of Chemistry and Physics*, 56th Edition, CRC Press, Boca Raton, FL (1975).
Webster, I. A., and M. L. Shuler, "Mathematical Models for Hollow-Fiber Enzyme Reactors," *Biotechnol Bioeng.*, **20**, 1541 (1978).
Youm, K. H., A. G. Fane, and D. E. Wiley, "Effects of Natural Convection Instability on Membrane Performance in Dead-End and Cross-Flow Ultrafiltration," *J. Membr. Sci.*, **116**, 229 (1996).

Appendix

Coefficients for the pressure Eqs. 10 and 11

The coefficients in the ECS and ICS pressure equations,

$$A_{r2}\frac{1}{r}\frac{\partial}{\partial r}\left(r\frac{\partial \hat{P}_S}{\partial r}\right)+A_{r1}\frac{\partial \hat{P}_S}{\partial r}+A_{\theta 2}\frac{1}{r}\frac{\partial^2 \hat{P}_S}{\partial \theta^2}+A_{\theta 1}\frac{1}{r}\frac{\partial \hat{P}_S}{\partial \theta}+A_{z2}\frac{\partial^2 \hat{P}_S}{\partial z^2}+A_{z1}\frac{\partial \hat{P}_S}{\partial z}+\hat{P}_S-\hat{P}_L=A_S \quad (10)$$

and

$$A_{L2}\frac{\partial^2 \hat{P}_L}{\partial z^2}-\hat{P}_L+\hat{P}_S=A_L \quad (11)$$

are defined as follows:

$$A_{r2}=-k_{S,r}\mu_S^{-1}\frac{A_{F1}}{A_{Lp}} \quad (A1)$$

$$A_{\theta 2}=-k_{S,\theta}\mu_S^{-1}\frac{1}{r}\frac{A_{F1}}{A_{Lp}} \quad (A2)$$

$$A_{z2}=-k_{S,z}\mu_S^{-1}\frac{A_{F1}}{A_{Lp}} \quad (A3)$$

$$A_{r1}=-\frac{k_{S,r}}{A_{Lp}}\left(F_1\mu_S^{-1}\frac{\partial \Delta\rho_S'}{\partial r}+F_\mu A_{F1}\frac{\partial \mu_S^{-1}}{\partial r}\right) \quad (A4)$$

$$A_{\theta 1}=-\frac{k_{S,\theta}}{A_{Lp}}\frac{1}{r}\left(F_1\mu_S^{-1}\frac{\partial \Delta\rho_S'}{\partial \theta}+F_\mu A_{F1}\frac{\partial \mu_S^{-1}}{\partial \theta}\right) \quad (A5)$$

$$A_{z1}=-\frac{k_{S,z}}{A_{Lp}}\left(F_1\mu_S^{-1}\frac{\partial \Delta\rho_S'}{\partial z}+F_\mu A_{F1}\frac{\partial \mu_S^{-1}}{\partial z}\right) \quad (A6)$$

$$A_S=-\Delta\Pi_{eff}-\varepsilon_S\frac{F_1}{A_{Lp}}\frac{\partial \Delta\rho_S'}{\partial t}+\frac{k_{S,r}}{A_{Lp}}\rho_0 g\sin\Psi\cos\theta\times\left[A_{F1}\frac{1}{r}\mu_S^{-1}\Delta\rho_S'+A_{F12}\mu_S^{-1}\frac{\partial \Delta\rho_S'}{\partial r}+F_\mu A_{F1}\Delta\rho_S'\frac{\partial \Delta\mu_S^{-1}}{\partial r}\right]-\frac{k_{S,\theta}}{A_{Lp}}\rho_0 g\sin\Psi\frac{1}{r}\left[A_{F12}\mu_S^{-1}\sin\theta\frac{\partial \Delta\rho_S'}{\partial \theta}\right.$$

$$+ A_{F1}\Delta\rho'_S\left(F_\mu \sin\theta \frac{\partial \mu_S^{-1}}{\partial \theta} + \mu_S^{-1}\cos\theta\right)\Bigg] - \frac{k_{S,z}}{A_{Lp}}\rho_0 g\cos\Psi\left[A_{F12}\mu_S^{-1}\frac{\partial \Delta\rho'_S}{\partial z} + F_\mu A_{F1}\Delta\rho'_S\frac{\partial \Delta\mu_S^{-1}}{\partial z}\right] \quad \text{(A7)}$$

$$A_{L2} = \rho'_L\frac{k_{L,z}}{\mu_L A_{Lp}} \quad \text{(A8)}$$

and

$$A_L = -\Delta\Pi_{eff} \quad \text{(A9)}$$

where

$$A_{F1} = 1 + F_1\Delta\rho'_S \quad \text{(A10)}$$

$$A_{F12} = 1 + 2F_1\Delta\rho'_S \quad \text{(A11)}$$

$$A_{Lp} = L_p A_V/\mu_0 \quad \text{(A12)}$$

In the equations above, μ_S^{-1} is the reciprocal viscosity of the ECS fluid; parameter F_μ has been introduced to conveniently neglect ($F_\mu = 0$) or include ($F_\mu = 1$) the ECS viscosity gradients; and parameter F_1 allows switching between the homogeneous ($F_1 = 0$) and inhomogeneous ($F_1 = 1$) forms of the ECS continuity equation; that is, Eqs. 4a and 4b can be represented by

$$F_1\left\{\varepsilon_S\frac{\partial \Delta\rho'_S}{\partial t} + \nu_{S,r}\frac{\partial \Delta\rho'_S}{\partial r} + \frac{\nu_{S,\theta}}{r}\frac{\partial \Delta\rho'_S}{\partial \theta} + \nu_{S,z}\frac{\partial \Delta\rho'_S}{\partial z} + \Delta\rho'_S\left[\frac{1}{r}\frac{\partial (r\nu_{S,r})}{\partial r} + \frac{1}{r}\frac{\partial \nu_{S,\theta}}{\partial \theta} + \frac{\partial \nu_{S,z}}{\partial z}\right]\right\} + \frac{1}{r}\frac{\partial (r\nu_{S,r})}{\partial r} + \frac{1}{r}\frac{\partial \nu_{S,\theta}}{\partial \theta} + \frac{\partial \nu_{S,z}}{\partial z} = \frac{L_p A_V}{\mu_0}(\hat{P}_L - \hat{P}_S - \Delta\Pi_{eff}) \quad \text{(A13)}$$

Manuscript received Feb. 4, 2003, and revision received Nov. 16, 2003.